Non-Gaussian Analysis of Diffusion-Weighted Imaging in Nasopharyngeal Carcinoma at 3T

Jing Yuan[1], Steven Kwok Keung Chow[1], David Ka Wai Yeung[1], Yujia Li[1], Anil T Ahuja[1], and Ann D King[1]

[1]*Imaging and Interventional Radiology, The Chinese University of Hong Kong, Shatin, NT, Hong Kong*

Introduction: Diffusion-weighted imaging (DWI) and the extracted apparent diffusion coefficient (ADC) based on the mono-exponential diffusion model have been widely studied and used for lesion detection, characterization and treatment response in head and neck (HN) region. However, water in biological tissues usually displays non-Gaussian diffusion behavior at extended b-value ranges that leads to the deviation of DWI signal fitting by using the mono-exponential diffusion model based on the Gaussian distribution assumption. Several non-Gaussian diffusion models [1-4] have been proposed to study the non-Gaussian diffusion behavior, but majorly in brain. The non-Gaussian models for HN-DWI analysis have rarely been explored [5]. The purpose of this pilot study is to investigate the feasibility of non-Gaussian diffusion models, including diffusion kurtosis imaging (DKI) [1], stretched exponential model (SEM) [2], intravoxel incoherent motion (IVIM) [3] and statistical model (STM) [4], for 3T DWI analysis in patients with nasopharyngeal carcinoma (NPC).

Methods: 16 patients with NPC received DWI scan at 3T using a fat-suppressed SE-EPI DWI sequence with a 16-channel HN coil (TR/TE=561ms/46ms, FA=90º, NSA=3, FOV=230mm, matrix=136x109, slices/thickness=5/4mm, b=0, 100, 200, 300, 400, 500, 600, 800, 100, 1200, 1400, 1500s/mm^2). Anatomical images were also acquired using fat-suppressed TSE sequences (TE/TR=80ms/4.5s, ETL=15, FOV=230mm, matrix=364x262). ROIs were drawn on primary tumors (PT, n=13) and metastatic nodes (MN, n=9) by a senior neuroradiologist (Fig. 1). Pixel-wise DWI signal in the ROIs were fitted by using the normal mono-exponential and non-Gaussian diffusion models. Mono-exponential ADC and non-Gaussian parameters maps within lesion ROIs were reconstructed (Fig. 2).

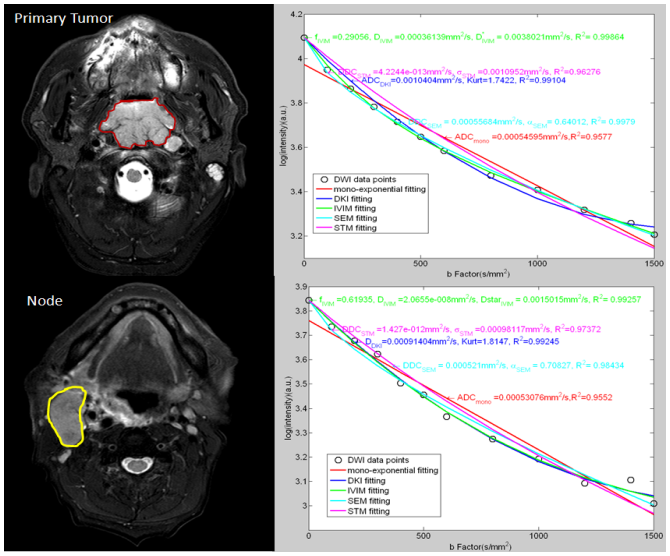

Fig.1. DWI signal fitting using the mono-exponential and non-Gaussian models

Results: Except for one MN, all PTs and MNs exhibited non-Gaussian diffusion behaviors at the extended b-value range up to 1500s/mm^2. All four non-Gaussian diffusion models obtained significantly better ($p<0.05$, F-test) goodness of fit for DWI signal fitting for both PTs and MNs (Fig. 1) than the mono-exponential model. The statistics of the extracted mono-exponential ADC and non-Gaussian parameters for PTs and MNs were listed in Table.1. Spearman correlation showed that $Kurt_{DKI}$, D_{IVIM}, D^*_{IVIM}, α_{SEM}, and ADC_{STM} had weak correlations with ADC_{mono} and may reveal new information about NPC lesion characteristics different from ADC_{mono}.

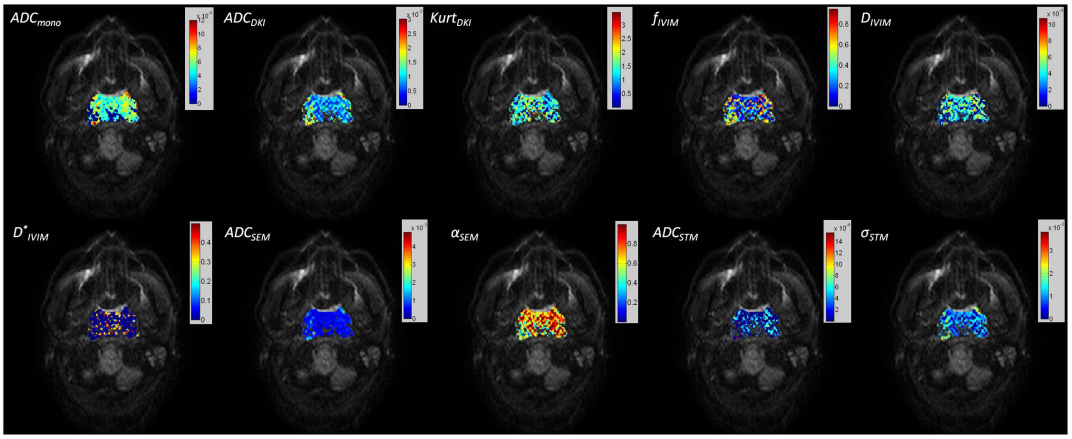

Fig.2. ADC_{mono} and non-Gaussian parameter maps in a NPC primary tumor (overlaid on the DWI image with b=0)

	ADC_{mono} (x10^{-3} mm^2/s)	ADC_{DKI} (x10^{-3} mm^2/s)	$Kurt_{DKI}$	f_{IVIM}	D_{IVIM} (x10^{-3} mm^2/s)	D^*_{IVIM} (x10^{-3} mm^2/s)	ADC_{SEM} (x10^{-3} mm^2/s)	α_{SEM}	ADC_{STM} (x10^{-3} mm^2/s)	σ_{STM} (x10^{-3} mm^2/s)
Primary Tumors	0.61±0.19	1.05±0.37	1.63±0.44	0.43±0.23	0.23±0.17	3.21±2.39	0.66±0.31	0.70±0.06	1.20e-5± 3.35e-5	1.20±0.56
Metastatic Nodes	0.54±0.11	0.95±0.28	1.76±0.29	0.40±0.24	0.21±0.19	3.30±2.21	0.55±0.19	0.69±0.07	2.46e-7± 4.25e-7	1.00e±0.33

Table 1. The statistics of the extracted mono-exponential ADC and non-Gaussian parameters for PTs and MNs

Discussion and Conclusion: The influence of the limited DWI SNRs at high b-values on the accuracy of signal fitting for non-Gaussian models should be further investigated in the future. The use of non-Gaussian modeling to fit DWI data acquired with an extended b range is feasible and yields significantly better fit than does mono-exponential modeling, and has potentials for lesion detection, characterization for NPC in future clinical practice.

Acknowledgement: This work is supported by HK GRC grant CUHK4660088 and SEG_CUHK02.

References: [1] Jensen JH et al, MRM 2005; 53:1432-40; [2] Bennett KM et al, MRM 2003; 50:727-34; [3] Le Bihan D et al, Radiology 1988; 168:497-505; [4] Yablonskiy DA et al. MRM 2003; 50:664-669; [5] Jansen JFA et al, AJNR 2010; 31:741-48